IEEE Transactions on Power Electronics (Volume: 38, Issue: 3, March 2023, pp 2811 - 2815) DOI: 10.1109/TPEL.2022.3217773



# A Piezoelectric-Resonator-Based DC-DC Converter Demonstrating 1 kW/cm$^3$ Resonator Power Density

Jessica D. Boles *Member, IEEE*, Joseph E. Bonavia *Student Member, IEEE*,
Jeffrey H. Lang *Life Fellow, IEEE* and David J. Perreault *Fellow, IEEE*

***Abstract*—Piezoelectric components hold promise for power conversion with unprecedented levels of power handling density at small size scales. Dc-dc converter topologies and operating modes have recently been established for high-efficiency utilization of piezoelectrics, and piezoelectric material selection and component design strategies have likewise been identified for high performance in power conversion. In this letter, we apply these developments to experimentally demonstrate the extraordinary power density capability of piezoelectrics. This 275-150 V, 12 W prototype achieves a piezoelectric resonator power handling density of 1.01 kW/cm$^3$ at 493 kHz, greatly exceeding the densities of previous designs and validating the significant miniaturization potential of piezoelectrics for power conversion.**

***Index Terms*—piezoelectric resonators, dc-dc power conversion**

## I. Introduction

Passive components, particularly magnetics (i.e., inductors and transformers), have long impeded the miniaturization of power electronics. Magnetics have fundamentally decreasing power densities and efficiencies at low volume [1], [2] but provide critical functionality for achieving efficient voltage regulation. Piezoelectric components, which store energy in the mechanical compliance and inertia of a piezoelectric material, have emerged as promising alternatives to magnetics for power conversion at small size scales [3], [4]. Piezoelectrics offer numerous advantages including high quality factors, high energy densities, galvanic isolation (with multi-port components), planar form factors, batch fabrication, and potential for integration.

Magnetic-less dc-dc converters based on piezoelectric resonators (PRs) have been demonstrated with high efficiency in [5]–[10]. These designs are based on recently-developed switching sequences and associated circuit topologies that maximize the PR's utilization across wide operating ranges; several of these are enumerated in [5]. Likewise, design tools including figures of merit for piezoelectric materials and vibration modes as well as guidelines for optimizing PR geometry for power conversion have been proposed in [11]. The framework of [11] reveals that – unlike magnetics – the power handling densities of PRs fundamentally increase at small scales.

In this letter, we combine these recent developments in topologies, switching sequences, material selection, and PR design criteria to experimentally demonstrate the power density promise of piezoelectrics. To the authors' knowledge, the resulting prototype achieves the highest PR power handling density of any PR-based dc-dc converter reported to date, and demonstrates the value of the aforementioned developments in enabling high power density.

J. D. Boles (jboles@mit.edu), J. E. Bonavia (jbonavia@mit.edu), J. H. Lang (lang@mit.edu), and D. J. Perreault (djperrea@mit.edu) are with the Massachusetts Institute of Technology (MIT), Cambridge, MA, USA. This material is based upon work supported by a gift from Texas Instruments, the National Science Foundation Graduate Research Fellowship (Grant No. 1122374), and the MIT Undergraduate Research Opportunities Program.

## II. Design Principles

To demonstrate the exceptional power density capability of piezoelectrics, we design a prototype converter with the objective of maximizing the PR's volumetric power handling density. This is achieved by combining (a) a maximum-efficiency circuit topology and switching sequence proposed in [5], with (b) a maximum-power-density PR design based on criteria for piezoelectric materials, vibration modes, and geometric dimensions developed in [11].

### A. Topology and Switching Sequence

Operating modes for PR-based dc-dc converters may be conceptualized in terms of switching sequences, or specific orderings of energy transfer stages and resonant stages throughout a switching period. Switching sequences for magnetic-less PR-based converters have been enumerated and downselected in [5] based on high-efficiency behaviors and practical characteristics. One of the highest-efficiency step-down switching sequences in this set is the $V_{in}$-$V_{out}$, *Zero*, $V_{out}$ sequence, named for the consecutive voltages $v_p$ of its energy transfer stages. This six-stage switching sequence can be realized with the topology of Fig. 1 and the waveforms of Fig. 2.

This switching sequence maintains high-efficiency behaviors such as soft charging of the PR's capacitance $C_p$, zero-voltage switching (ZVS), all-positive instantaneous power transfer, and minimal charge circulation across wide operating ranges. This switching sequence likewise maintains constant theoretical efficiency for a given $V_{in}$ and $P_{out}$ in the $\frac{1}{2} < \frac{V_{out}}{V_{in}} < 1$ voltage conversion range, allowing for high-efficiency regulation of $V_{out}$. The PR's amplitude of resonance (i.e., the amplitude $I_L$ of its assumed-sinusoidal $i_L$ in Fig. 1) for this sequence and operating region can be modeled as [5]:

$$I_L = \pi \left( \frac{P_{out}}{V_{in}} + f C_p V_{in} \right) \quad (1)$$

for which $P_{out}$ is the power delivered to the load, $f$ is the switching frequency, and $V_{in}$ and $C_p$ are as defined in Fig. 1.

We adopt the $V_{in}$-$V_{out}$, *Zero*, $V_{out}$ switching sequence and its corresponding topology in Fig. 1 for this prototype; more analysis of its operation can be found in [5].

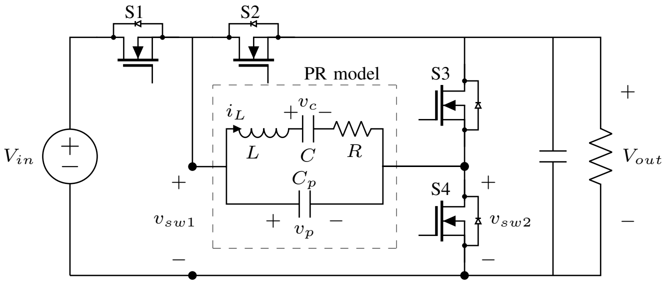


Fig. 1. Topology corresponding to the $V_{in}$-$V_{out}$, *Zero*, $V_{out}$ switching sequence proposed in [5]. The PR is represented with the Butterworth-Van Dyke model for operation near its fundamental resonance [12].

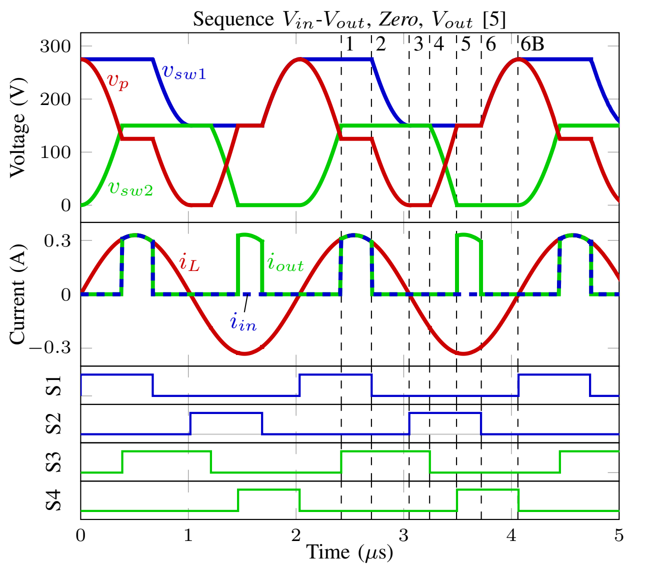


Fig. 2. Simulated waveforms for switching sequence $V_{in}$-$V_{out}$, *Zero*, $V_{out}$ with PR parameters in Table II. $V_{in}$ = 275 V, $V_{out}$ = 150 V, $P_{out}$ = 12 W.

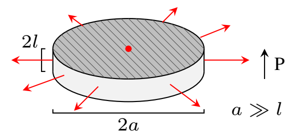


$$C_p = \varepsilon_{33}^T(1-k_p^2)\frac{\pi a^2}{2l}$$
$$C = C_p\frac{k_p^2}{1-k_p^2}\frac{2(1+\sigma)}{\kappa_{o,r}^2-(1-\sigma^2)}$$
$$L = \frac{a^2}{2v_a^2 C_p}\frac{1-k_p^2}{k_p^2}\frac{\kappa_{o,r}^2-(1-\sigma^2)}{\kappa_{o,r}^2(1+\sigma)}$$
$$R = \frac{1}{Q_m}\sqrt{\frac{L}{C}}$$

Fig. 3. Example illustration of the radial vibration mode with electrodes denoted by shaded areas, displacement directions marked with red arrows, and the material's polarization direction shown with 'P'. Circuit model parameters are provided in terms of material properties defined in Table I [13].

## B. Piezoelectric Resonator

The performance of a PR can vary widely based on its material, vibration mode, geometric dimensions, electrode pattern, mechanical mounting structure, and electrical contacts. A typical first step in the PR design process is co-selection of a material and intended vibration mode. Figures of merit (FOMs) for piezoelectric materials and vibration modes have been derived in [11] based on the highest-efficiency switching sequence detailed in Section II-A. One promising material and mode combination for high volumetric power density is the PZT radial mode, which has an extremely high FOM for volumetric energy handling density (i.e., power density normalized to frequency) and an acceptably high FOM for mechanical efficiency. The radial vibration mode is visualized in Fig. 3, and its mechanical efficiency FOM ($\text{FOM}_M$) is

$$\text{FOM}_M = \left(\frac{P_{out}}{P_{loss}}\right)_{max} = \frac{1}{2\pi^2 B_o R_o} \tag{2}$$

where $B_o = \varepsilon_{33}^T(1-k_p^2)\frac{\bar{\kappa}_o v_a}{4\pi}$ and $R_o = \frac{\kappa_{o,r}^2-(1-\sigma^2)}{Q_m k_p^2 \varepsilon_{33}^T v_a \kappa_{o,r}(1+\sigma)}$ for which material properties are defined in Table I.

Besides its FOMs, the radial vibration mode is also advantageous in that (a) it is the lowest-frequency mode for a circular disc, which minimizes the presence of spurious modes[1] in the PR's inductive frequency region, and (b) its necessary shape for maximum efficiency is more planar than that of other modes[2], providing more surface area for heat extraction. Discrete radial-mode PZT components are also widely available and have been demonstrated with high efficiency in multiple power converter designs to date [5], [8], [9], [11]. We therefore adopt the PZT radial mode for this prototype; more analysis of its characteristics can be found in [11].

TABLE I
PIEZOELECTRIC MATERIAL PROPERTIES AND TYPICAL PZT VALUES

| Symbol | Name | APC 841 Value* |
|---|---|---|
| $Q_m$ | Mechanical Quality Factor | 1400 |
| $k_p$ | Electromechanical Coupling Factor | 0.6 |
| $\varepsilon_{33}^T$ | Permittivity at Constant Stress | 12.2 nF/m |
| $v_a$ | Acoustic Velocity | 3.07 km/s |
| $\sigma$ | Poisson's Ratio | 0.395 |
| $\kappa_{o,r}$ | Normalized Wave Number at $f_r$ | 2.11 |
| $\bar{\kappa}_o$ | Normalized Wave Number at Maximum Efficiency | 2.28 |

*$Q_m$, $k_p$, and $\varepsilon_{33}^T$ are provided by [14]. Others are calculated as in [11], [13].

The FOMs proposed in [11] correspond to PR geometry design conditions for achieving both maximum efficiency and maximum energy handling density at a desired converter operating point. These geometry conditions may also be applied to find the converter operating points that maximally utilize a given PR. For a PR operating in the radial mode, the $V_{in}$ and $P_{out}$ corresponding to maximum efficiency and loss-limited volumetric energy handling density are:

$$V_{in} = \sqrt{\frac{al \cdot H \cdot \text{FOM}_M}{B_o}} \tag{3}$$

$$P_{out} = \pi a^2 \cdot H \cdot \text{FOM}_M \tag{4}$$

where $H$ is the PR's areal loss density (i.e., $\frac{P_{loss}}{\pi a^2}$) and describes the PR's thermal management requirement assuming most heat extraction occurs through its electrode surface(s). Thus, maximum loss-limited energy handling density is set by the maximum $H$ that a PR's thermal design can accommodate. For lower values of $H$, maximum efficiency can still be

[1]Spurious modes (i.e., minor resonant modes that increase loss) are often higher-order harmonics of a component's lower-frequency vibration modes.

[2]The radial vibration mode is one of several "perpendicular" vibration modes as defined in [11], which tend to require more planar shapes than "parallel" vibration modes for maximum efficiency.

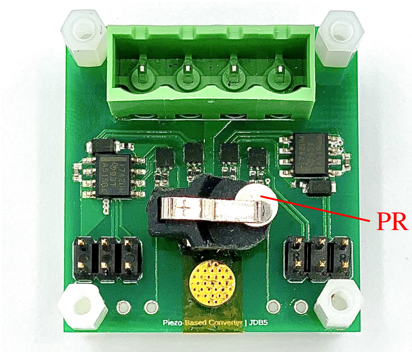


Fig. 4. Experimental prototype based on the topology of Fig. 1 with an APC International PR (part 186: APC 841 material, $2a$ = 4.75 mm, $2l$ = 0.67 mm) mounted with a Keystone Electronics coin battery holder (part 500). All switches are EPC2012C GaN FETs, located under the PR mount on the board. Gate circuitry includes Texas Instruments UCC27611 gate drivers and ISO7420MD digital isolators.

achieved for any $V_{in}$ and $P_{out}$ that satisfy (3)-(4). We note that these relationships for other vibration modes, stress-limited density, or electric-field-limited density can also be derived from the framework of [11].

While these analyses assume ideal switching devices, the presence of significant switch capacitance can be detrimental to a PR's efficiency and power density capability. Switch capacitance also requires resonance between energy transfer stages for ZVS, necessitating more PR charge displacement for the same $P_{out}$. Switch capacitance may be integrated into (2)-(4) above by substituting $B_o$ for $B_{o+sw}$, where

$$B_{o+sw} = (1 + \frac{2C_{oss}}{C_p})B_o \tag{5}$$

and $C_{oss}$ equals the effective switch capacitance. Thus, the impact of switch capacitance on achievable efficiency and power density is minimized as $\frac{2C_{oss}}{C_p} \to 0$.

## III. Converter Prototype

As a case study, we confine this prototype to off-the-shelf piezoelectric components and evaluate candidates according to their power densities at their maximum-utilization operating points in (3) and (4). This calculation assumes $H$ = 1 W/cm$^2$ and considers suitable switch capacitance, requiring co-selection of a switching device capable of supporting the suggested $V_{in}$ in (3) with minimal capacitance compared to $C_p$. We select the APC International part 186 (APC 841 disc[3], $2a$ = 4.75 mm, $2l$ = 0.67 mm) with EPC2012C FETs for this prototype; the analysis of Section II-B suggests this combination to be capable of 1 kW/cm$^3$ PR power handling density at $V_{in}$ = 275 V and $P_{out}$ $\approx$ 12 W.

As pictured in Fig. 4, we implement this design on a two-layer 1-oz copper printed circuit board with the parts listed in Fig. 4's caption. For this size PR, traditional mounting structures present considerable trade-offs: solder joints provide a reliable electrical connection but degrade $Q_m$ if too large and break if too small, and spring mounts provide high $Q_m$ but scratch the electrode if too tight and lose electrical connection if too loose. For demonstration purposes, the PR in this prototype is mounted with a modified coin battery holder (Keystone Electronics part 500), which provides a reliable electrical connection with a wide contact point and an acceptable degradation of $Q_m$. We note that this structure permits lateral PR movement, and the PR settles to the position shown in Fig. 4 upon initial converter operation.

[3]Although other materials considered in [11] have higher theoretical FOM$_M$, we select APC 841 for its high experimental efficiency demonstrated in [11] and its wide availability in off-the-shelf parts.

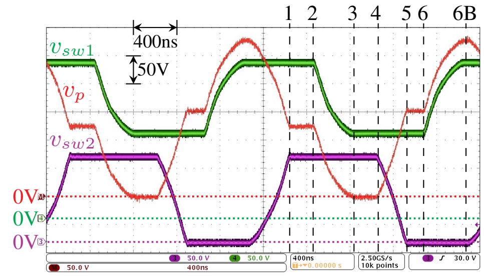


Fig. 5. Experimental waveforms at $V_{in}$ = 275 V, $V_{out}$ = 150 V, $P_{out}$ = 12 W, and $f$ = 493 kHz with the prototype pictured in Fig. 4.

TABLE II
Characterized Prototype Model Parameters

| $C_{p+par}$ | $L$ | $C$ | $R$ | $Q_m$ | $k_p$ | $\kappa_{o,r}$ | $\bar{\kappa}_o$ |
|---|---|---|---|---|---|---|---|
| 457 pF | 1.51 mH | 75.2 pF | 4.45 Ω | 1030 | 0.424 | 2.05 | 2.13 |

For all experiments, we operate this converter with a constant-voltage load and forced convection of 300 LFM using a server fan (Nidec part M33406-55G10). We control the converter with open-loop switching times, which we manually tune at each operating point for the switching sequence's high-efficiency behaviors discussed in Section II-A. Control handles for tuning include frequency, duty cycle of each half-bridge, phase shift between half-bridges, and dead time, and there is one unique tuning point at which all of the sequence's high-efficiency behaviors are achieved for a given $V_{in}$, $V_{out}$, and $P_{out}$. The result is the experimental waveforms shown in Fig. 5, which compare closely in form with those in Fig. 2.

## IV. Experimental Results

To contextualize this prototype's performance, we conduct a small-signal characterization of the PR mounted in this fully-assembled prototype using an impedance analyzer with no bias voltage. A frequency sweep throughout the PR's inductive region is shown in Fig. 6a, revealing near-ideal smoothness except for one discontinuity at 495 kHz. This discontinuity causes the equivalent series resistance and phase to locally increase and decrease, respectively. Fitting the Butterworth-Van Dyke equivalent circuit to this impedance curve yields the parameters shown in Table II, though we note that $C_{p+par}$ is an overestimate since switch capacitance decreases with respect to bias voltage. The PR's $Q_m$, $k_p$, $\kappa_{o,r}$, and $\bar{\kappa}_o$ are characterized as described in [11], [13] and translate to an expected maximum PR efficiency of 98.2% at 491 kHz.

We test this converter's power stage efficiency vs. $P_{out}$ for three different input/output voltage levels, each with the same conversion ratio, and Fig. 6b displays the results. This converter achieves competitive efficiency across a wide operating range and a full load efficiency of 93.3%. The maximum

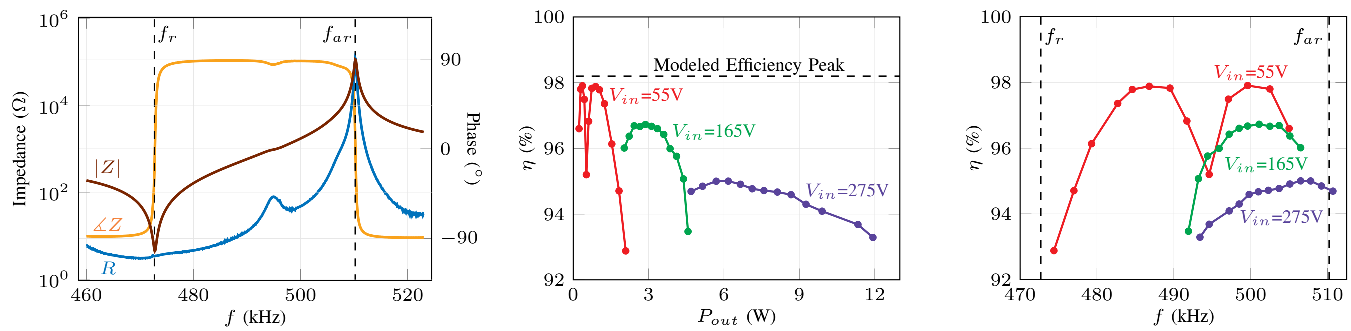


(a) (b) (c)

Fig. 6. (a) Small-signal impedance characteristic of the PR in the fully-assembled prototype pictured in Fig. 4, obtained after experiments to capture the PR's steady-state position in the mounting structure. Corresponding circuit model parameters are provided in Table II. (b) Experimental power-stage efficiency vs. $P_{out}$ for various $V_{in}$ (marked) each with $V_{out} = \frac{6}{11}V_{in}$; same data as Fig. 6c. (c) Experimental power-stage efficiency vs. $f$ for various $V_{in}$ (marked) each with $V_{out} = \frac{6}{11}V_{in}$; same data as Fig. 6b. Efficiencies do not consider auxiliary power.

observed efficiency for the lowest voltage level ($V_{in} = 55$ V) approaches the theoretical maximum PR efficiency of 98.2%. However, maximum efficiency is observed to be lower for higher voltage levels, which correspond to greater $I_L$. This dependence on excitation level is a departure from the framework described in Section II, in which maximum efficiency is a function of only $Q_m$ and material properties. This suggests the piezoelectric component's material properties and/or loss characteristics to be nonlinear with respect to excitation level.

Fig. 6c plots these efficiency curves with respect to frequency, further highlighting the aforementioned discrepancies between voltage levels. The downward efficiency spikes between 491 kHz and 495 kHz may be attributed to the impedance discontinuity shown in Fig. 6a. The $V_{in} = 55$ V efficiency characteristic rebounds from this spike at lower frequencies, suggesting that the $V_{in} = 165$ V and $V_{in} = 275$ V efficiencies may do the same if operated at lower frequency (and therefore higher power).

Previous reports for PR power handling density in [6], [9], [10] have considered only the component's "active" volume between its electrodes, in which most energy is assumed to be stored. This does not consider the component's mounting structure (including "inactive" material used for anchoring) or electrical connections, as these aspects of PR design are yet to be optimized for power conversion. Adopting this standard, this prototype achieves a piezoelectric component power handling density of 1.01 kW/cm$^3$. We validate the stability of this operating point with ten minutes of continuous operation, during which the prototype maintains the same waveforms without need to adjust its open-loop switching times. After this ten-minute period, the PR is thermally stable at <36 °C with forced convection of 300 LFM.

## V. Conclusion

The observed piezoelectric component power handling density of 1.01 kW/cm$^3$ represents a substantial increase over other recent piezoelectric-based dc-dc converter prototypes, which report 148 W/cm$^3$ [6], 176.8 W/cm$^3$ [9], and 128 W/cm$^3$ [10]. All four prototypes are based on the same family of high-efficiency switching sequences, so the density increase may be attributed to this prototype's high-energy-handling-density PR design according to the FOMs and geometry conditions in [11]. This marks a significant milestone in demonstrating the power density capabilities of piezoelectrics and their miniaturization potential for power conversion.

## References


[1] C. R. Sullivan, B. A. Reese, A. L. Stein, and P. A. Kyaw, "On size and magnetics: Why small efficient power inductors are rare," in *Proc. IEEE Intl. Symposium on 3D Power Electronics Integration and Manufacturing*, Raleigh, NC, USA, Jun. 2016, pp. 1–23.

[2] D. J. Perreault, J. Hu, J. M. Rivas, Y. Han, O. Leitermann, R. C. Pilawa-Podgurski, A. Sagneri, and C. R. Sullivan, "Opportunities and challenges in very high frequency power conversion," in *Proc. IEEE Applied Power Electronics Conference and Exposition*, Washington, DC, USA, Feb. 2009, pp. 1–14.

[3] P. A. Kyaw, A. L. Stein, and C. R. Sullivan, "Fundamental examination of multiple potential passive component technologies for future power electronics," *IEEE Transactions on Power Electronics*, vol. 33, no. 12, pp. 10,708–10,722, 2018.

[4] J. D. Boles, J. J. Piel, E. Ng, , J. E. Bonavia, J. H. Lang, and D. J. Perreault, "Piezoelectric-based power conversion: Recent progress, opportunities, and challenges," in *Proc. IEEE Custom Integrated Circuits Conference*, Newport Beach, CA, Apr. 2022, pp. 1–8.

[5] J. D. Boles, J. J. Piel, and D. J. Perreault, "Enumeration and analysis of dc-dc converter implementations based on piezoelectric resonators," *IEEE Transactions on Power Electronics*, vol. 36, no. 1, pp. 129–145, 2021.

[6] W. Braun, E. Stolt, L. Gu, J. J. Segovia-Fernandez, S. Chakraborty, R. Lu, and J. M. R. Davila, "Optimized resonators for piezoelectric power conversion," *IEEE Open Journal of Power Electronics*, 2021.

[7] E. Stolt, W. D. Braun, L. Gu, J. Segovia-Fernandez, S. Chakraborty, R. Lu, and J. Rivas-Davila, "Fixed-frequency control of piezoelectric resonator dc-dc converters for spurious mode avoidance," *IEEE Open Journal of Power Electronics*, vol. 2, pp. 582–590, 2021.

[8] B. Pollet, G. Despesse, and F. Costa, "A new non-isolated low power inductorless piezoelectric dc-dc converter," *IEEE Transactions on Power Electronics*, vol. 34, no. 11, pp. 11 002–11 013, 2019.

[9] M. Touhami, G. Despesse, and F. Costa, "A new topology of dc-dc converter based on piezoelectric resonator," *IEEE Transactions on Power Electronics*, 2022.

[10] M. Touhami, G. Despesse, T. Hilt, M. Bousquet, A. Reinhardt, E. Borel, V. Breton, K.-F. Gneza, and F. Costa, "Piezoelectric materials for the dc-dc converters based on piezoelectric resonators," in *Proc. IEEE Workshop on Control and Modelling of Power Electronics (COMPEL)*. Cartagena de Indias, Columbia: IEEE, Nov. 2021, pp. 1–8.

[11] J. D. Boles, J. E. Bonavia, P. L. Acosta, Y. K. Ramadass, J. H. Lang, and D. J. Perreault, "Evaluating piezoelectric materials and vibration modes for power conversion," *IEEE Transactions on Power Electronics*, 2022.

[12] K. S. Van Dyke, "The piezo-electric resonator and its equivalent network," *Proceedings of the Institute of Radio Engineers*, vol. 16, no. 6, pp. 742–764, 1928.

[13] J. Erhart, P. Půlpán, and M. Pustka, *Piezoelectric Ceramic Resonators*. Springer, 2017.

[14] "Physical and piezoelectric properties of APC materials". APC International, Ltd. [Online]. Available: https://www.americanpiezo.com/apc-materials/physical-piezoelectric-properties.html